Modern Physics Letters A
© World Scientific Publishing Company

arXiv:hep-ph/0312127v2 10 Dec 2003

# MEDIUM-INDUCED GLUON RADIATION AND JET QUENCHING IN HEAVY ION COLLISIONS.

CARLOS A. SALGADO
*Theory Division, CERN*
*CH-1211 Geneva 23, Switzerland*
*carlos.salgado@cern.ch*

In this brief review, I summarize the new developments on the description of gluon radiation by energetic quarks traversing a medium as well as the observable consequences in high-energy heavy ion collisions. Information about the initial state is essential for a reliable interpretation of the experimental results and will also be reviewed. Comparison with experimental data from RHIC and expectation for the future LHC will be given.

*Keywords*: Jet Quenching, Heavy Ion Collisions, Jets

PACS Nos.: 25.75.-q, 12.38.Mh, 24.85.+p

## 1. Introduction

The experimental program on high energy heavy ion collisions attempts to study the behavior of QCD matter under extreme conditions. The original, and still most important goal, is the creation and characterization of the quark-gluon plasma, a thermalized state of deconfined quarks and gluons that could be the form of matter of the whole Universe only several $\mu s$ after the Big-Bang. The study of high-$p_t$ processes as probes of the produced medium starts with the seminal work of J.D. Bjorken in 1982 [1]. The idea was that if a medium is produced in a collision, the high-$p_t$ particles produced inside the medium in the initial stage would loss energy (and eventually thermalize) when escaping it. The arguments in [1] were based on elastic scattering, and the loss turned out to be too small. Later refinements [2,3,4] propose the medium-induced gluon radiation as the dominant source of energy loss.

Twenty years latter, in the heavy ion collider era started with RHIC, these effects could be measured for the first time. The new experimental facts coming from RHIC when comparing central AuAu with pp collisions are the following: the suppression of particles with high-$p_t$ [8,9,10] (independent of the particle species for $p_t \gtrsim 4$ GeV) and the total extinction of the signal associated to a high-$p_t$ particle in the backward hemisphere [11] (back-to-back correlations). Together with this, experimental data in dAu collisions find an enhancement of high-$p_t$ particle production [10,12,13,14] (the so-called Cronin effect) and back-to-back correlations of the same magnitude as the ones measured in pp collisions [13]. These effects point to a strong interaction

of the high-$p_t$ particle with the (dense) produced medium in agreement with the *jet quenching* scenario. In the following we will present the general formalism, based on collinear factorization, in which most of the present calculations are based as well as some comparison with experimental data.

To leading order in perturbative QCD, high-$p_t$ hadroproduction in proton–proton collisions is described by the factorization formula (see e.g. [15]):

$$E\frac{d\sigma^h}{d^3p} = K(\sqrt{s}) \int dz dx_1 dx_2 \frac{\hat{s}}{\pi z^2} \delta(\hat{s}+\hat{t}+\hat{u}) \times \\ \times \sum_{i,j} f_i^A(x_1,Q^2)\, f_j^B(x_2,Q^2)\, \frac{d\sigma^{ij\to k}}{d\hat{t}}\, D_{k\to h}(z,Q^2), \tag{1}$$

where $f_i^A$, $f_j^B$ are the proton parton distribution functions (PDF), $d\sigma^{ij\to k}/d\hat{t}$ is the partonic cross section and $D_{k\to h}(z,Q^2)$ describes the fragmentation of a parton $k$ into the hadron $h$ carrying a fraction $z$ of the momentum. The description of the experimental data by (1) is very reasonable [15,16,17].

In the case of heavy ion collisions, both the initial and, possibly, the final state are different. Indeed, the nuclear parton distributions are different from those in free protons and the eventually produced medium would modify the fragmentation. The knowledge of the PDF for bounded nucleons gives the baseline for the final state effects which would provide the information about the medium. So, the first goal is to obtain these nuclear PDF from experimental data in different processes.

The review is organized as follows: in next section we give a description of the initial state effects in terms of nuclear modifications of PDF; Section 3 describes the medium-induced gluon radiation spectrum, which is the main part of the present work; in Section 4 some applications are discussed, both for inclusive particle production (where a comparison with RHIC data is possible) as well as for the more differential case of jet observables. In the last two sections we comment on different approaches and give our conclusions.

## 2. Initial state effects: shadowing

Nuclear and free proton PDF – $f_i^A$ and $f_i^p$ respectively – are normally related by the ratio $R_i^A$

$$f_i^A(x,Q^2) = R_i^A(x,Q^2) f_i^N(x,Q^2)\,. \tag{2}$$

For the corresponding ratio of the structure function $F_2$ several different regions have been measured, as shadowing ($R_{F_2}^A < 1$) at small values of $x$, antishadowing ($R_{F_2}^A > 1$) for intermediate $x$ and EMC ($R_{F_2}^A < 1$) and Fermi motion for large $x$. In this way, a similar structure is expected for the nuclear PDF $f_i^A(x,Q^2)$

The proton PDF are usually obtained in global fits to experimental data in well established DGLAP analysis[18,19]. The main difficulty in applying the same method to the nuclear case is the lack of experimental data. In this section we present two

sets of nuclear PDF (EKRS [20] and HKM [21])[a] and comment about the experimental constraints to the different flavors, specially those for gluons.

### 2.1. *EKRS analysis of nuclear PDF*

The goal of nuclear DGLAP analyzes is to obtain a set of nuclear PDF following the procedure of the proton case. Namely, fixing the initial parton distributions at a $Q_0^2 \gg \Lambda_{QCD}^2$ and evolving them to larger $Q^2$ values by DGLAP equations. The comparison with data would fix the free parameters in the initial condition. In practice, what is usually done is to obtain the initial *ratios*, $R_i(x, Q_0^2)$ for different partons $i$, and use a known set of proton PDF (as MRST [18], CTEQ [19], etc...) to obtain the nuclear PDF. In the EKRS analysis, data on nuclear $F_2$, and DY measured in pA collisions is used. Further constraints are momentum and baryon number sum rules. At the initial scale, the ratios for valence $R_V(x, Q_0^2)$ (same for $u_V$ and $d_V$), sea $R_S(x, Q_0^2)$ (same for $\bar{u}$, $\bar{d}$ and $\bar{s}$) and gluons $R_g(x, Q_0^2)$ are obtained in the following way:

• At large values of $x$ ($x \gtrsim 0.3$), $R_{F_2}$ data is used to fix the valence quarks ratio $R_V$. Both $R_S$ and $R_g$ are not constrained, so they are assumed to be equal to $R_V$.

• At intermediate values of $x$ ($0.04 \lesssim x \lesssim 0.3$) both DIS and DY data constrain the ratios $R_V$ and $R_S$. Baryon number sum rule imposes also constraints to valence ratio. In this region, the gluon ratio is fixed by momentum sum rule, with the help of NMC data [24] to fix the value of $x$ where $R_g(x)$=1 (see below). This produces a large gluon antishadowing.

• At small values of $x$ ($x \lesssim 0.04$), $R_S = R_{F_2}$ and a saturation of $R_{F_2}$ is assumed for $x \lesssim 10^{-3}$; $R_g = R_{F_2}$ is taken for the very small $x$ values – notice that evolution modifies this equality; $R_V$ is fixed by baryon number sum rule.

Once the initial conditions are known, LO-DGLAP evolution is performed, and the parameters of the initial conditions fixed by comparing to data at different values of $Q^2$. The initial conditions obtained by this method are plotted for a Pb nucleus in Fig. 2.1 and compared with HKM [21]. The main differences come from the fact that HKM do not use data on Drell-Yan [25] with nuclei (essential to constrain valence and sea quarks at intermediate $x$) nor the $Q^2$-dependent data measured by NMC [24].

### 2.2. *Constraints for gluons*

At LO, the gluon distribution does not directly contribute to the DIS or DY cross sections. It instead drives the $Q^2-$evolution of all other flavors: at small values of

[a]By the time this review was finished a new analysis was published [22]. Quantitative differences appear for the gluons when compared with EKRS but the qualitative features are in agreement with this set. (See Ref. [22] for further details and the effect of these corrections on the high-$p_t$ $\pi^0$ yields measured at RHIC. See also [23] for a related approach).

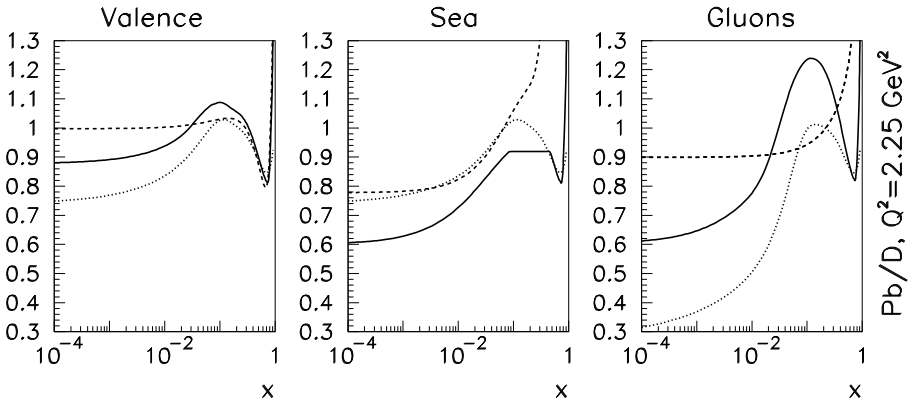


Fig. 1. EKS98 (solid lines) and HKM (dashed lines) initial conditions for the ratios of valence, sea and gluon PDF of Pb over deuterium. Also shown are the corresponding ratios for the new HIJING parametrization (dotted lines).

$x$, DGLAP at LO gives $\partial F_2^{p(n)}/\partial \log Q^2 \sim xg(2x, Q^2)$. So, for the ratios,

$$\partial R_{F_2}^A(x, Q^2)/\partial \log Q^2 \propto \left\{ R_g^A(2x, Q^2) - R_{F_2}^A(x, Q^2) \right\}. \tag{3}$$

In order to obtain a positive $\log Q^2$-slope, as measured by the NMC Collaboration [24] (see Fig. 2) a very strong gluon shadowing for $x \gtrsim 0.01$ is not allowed by (3). To quantify this statement [26], we have applied DGLAP evolution to different initial conditions and compare with the NMC data, the comparison is done in Fig. 2. The slopes reflect the gluon distribution, in particular, the negative slopes obtained when taken new HIJING parametrization [27] indicate that the very strong shadowing for gluons is in disagreement with data. (This is, also, in agreement with the new analysis [22]).

Summarizing, in order to use the collinear factorization formula (1) a set of nuclear PDF is needed. These nuclear PDF can be constrained by DIS and DY experimental data and evolved by DGLAP equations. In this framework, a strong gluon shadowing for $x \gtrsim 0.01$ is not supported by present data. EKRS parametrization gives[15], for RHIC at $y \sim 0$, a moderate enhancement in the intermediate region of $p_t$, but interestingly, in agreement with the increase in the $\pi^0$ yield measured in dAu collisions [12].

## 3. Final-state effects: medium-induced gluon radiation

The medium-induced distribution of gluons of energy $\omega$ radiated off an initial hard parton has been computed by several methods and approximations [3,4,5,6]. They

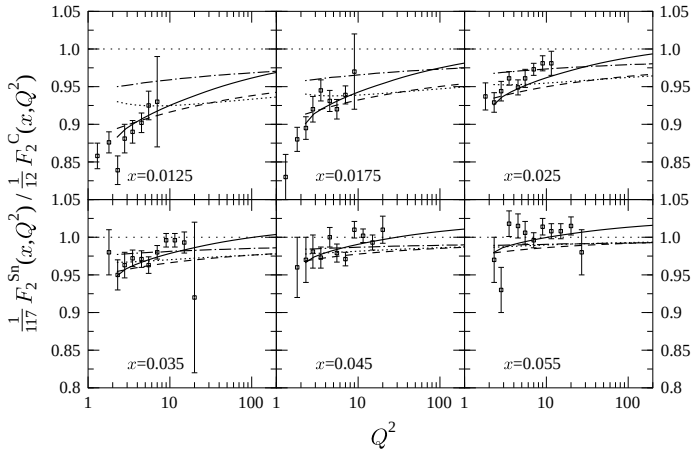


Fig. 2. $Q^2$-evolution of the ratios of $F_2$ in Sn and C for different initial conditions EKS98 [20] (solid lines), HKM [21] (dotted-dashed lines), HPC [28] (dashed lines) and new HIJING [27] (dotted lines) compared with the NMC results.

can be obtained as particular cases of the general $k_t$-differential spectrum [6,7]

$$\omega \frac{dI}{d\omega\, d\mathbf{k}} = \frac{\alpha_s\, C_R}{(2\pi)^2\, \omega^2}\, 2\mathrm{Re} \int_0^\infty dy_l \int_{y_l}^\infty d\bar{y}_l \int d^2\mathbf{u}\, e^{-i\mathbf{k}_t\cdot\mathbf{u}}\, e^{-\frac{1}{2}\int_{\bar{y}_l}^\infty d\xi\, n(\xi)\,\sigma(\mathbf{u})} \times$$
$$\times \frac{\partial}{\partial \mathbf{y}} \cdot \frac{\partial}{\partial \mathbf{u}} \int_{\mathbf{y}=\mathbf{r}(y_l)}^{\mathbf{u}=\mathbf{r}(\bar{y}_l)} \mathcal{D}\mathbf{r} \exp\left[ i \int_{y_l}^{\bar{y}_l} d\xi \frac{\omega}{2} \left( \dot{\mathbf{r}}^2 - \frac{n(\xi)\,\sigma(\mathbf{r})}{i\,2\,\omega} \right) \right] . \qquad (4)$$

Here, $C_R$=$C_F$=4/3 for quarks and $C_R$=$C_A$=3 for gluons. Medium properties enter (4) via the product of the medium density $n(\xi)$ of scattering centers times the dipole cross section $\sigma(\mathbf{r})$ which measures the interaction strength of a single elastic scattering. The solution for a general $n(\xi)\sigma(\mathbf{r})$ is unknown, and two approximations have been studied up to now: the multiple soft scattering limit, $n(\xi)\,\sigma(\mathbf{r}) \approx \frac{1}{2}\hat{q}(\xi)\,\mathbf{r}^2$, in which the path integrals reduce to those of a harmonic oscillator and can be solved analytically – this is the approximation used by the BDMPS group [3] and Zakharov [4]; the single hard scattering limit, which consists in a series expansion in $n(\xi)\sigma(\mathbf{r})$, where $\sigma(\mathbf{r})$ is modeled by a Yukawa potential with Debye screening mass $\mu$ – this is the approximation used by the GLV group [5].

Eq. (4) implies a one-to-one correspondence between the average energy loss of the parent parton, and the transverse momentum broadening of the associated gluon radiation, as argued in Ref. [29]. In Fig. 3 we present the numerical results of $\omega dI/d\omega\, d\mathbf{k}$ for quarks in the two approximations.

Most of the qualitative properties of the medium-induced gluon radiation spectrum can be understood by coherence arguments. Let us concentrate on the multiple soft scattering approximation, the same arguments hold for the single hard with the

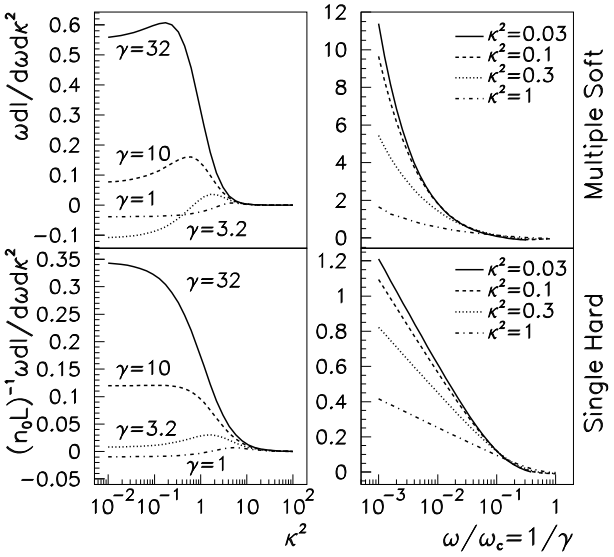


Fig. 3. The gluon energy distribution (4) as a function of the rescaled gluon energy $\omega/\omega_c$ and the rescaled gluon transverse momentum $\kappa$, see eq. (6). ($\alpha_s$=1/3 has been taken).

change $\hat{q} \rightarrow \mu^2/L$. For a gluon emitted with energy $\omega$ and transverse momentum $k_t$, the phase and the gluon formation time are

$$\varphi = \left\langle \frac{k_t^2}{2\omega}\,\Delta z \right\rangle \Longrightarrow l_{coh} \sim \frac{\omega}{k_t^2}\,. \tag{5}$$

The medium is characterized by the transport coefficient $\hat{q} \simeq \frac{\mu^2}{\lambda}$, giving the average transverse momentum $\mu^2$ transfered from the medium to the gluon per mean free path $\lambda$. So, $k_t^2 \sim \mu^2 l_{\rm coh}/\lambda$, when $l_{\rm coh}$ reaches the length of the medium $L$ one has $k_t^2 \sim \hat{q}L$. So, this is a maximum for the $k_t$ of the emitted gluon. If one defines

$$\kappa^2 = \frac{k_t^2}{\hat{q}L}\ ,\ \omega_c = \frac{1}{2}\hat{q}L^2 \qquad \left[\kappa^2 = \frac{k_t^2}{\mu^2}\ ,\ \omega_c = \frac{1}{2}\mu^2 L\ \ \text{For Single Hard}\right], \tag{6}$$

the phase for $\Delta z = L$ is $\varphi \sim \kappa^2\ \omega_c/\omega$. The radiation can only be formed when $\varphi \gtrsim 1$, so a suppression of the radiation appears when $\kappa^2 \lesssim \omega_c/\omega$. The plateau at small values of $\kappa$ for fixed $\omega/\omega_c$ in Figure 3 is due to these coherence effects. Moreover, at large values of $\omega \gtrsim \omega_c$ the spectrum is also suppressed. This is the well known LPM suppression first discussed by the BDMPS group [3]. These features are characteristic of QCD as the multiple scattering is performed by the (eventually) emitted gluon in the high-energy approximation. In the case of QED, the photon does not interact and the relevant phase contains now the energy of the electron instead of $\omega$.

For practical applications, the $k_t$-integrated spectrum is needed. The kinematical limits $0 < k_t < \omega$ are imposed to compute the spectra of Fig. 4 for different values

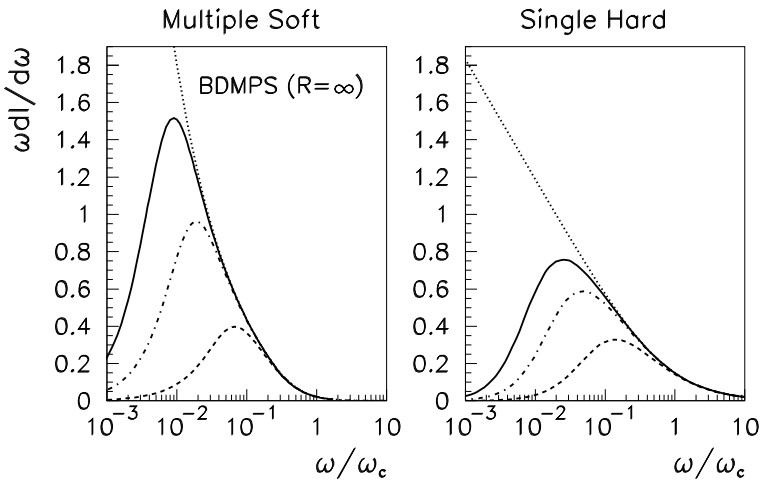


Fig. 4. The medium-induced gluon energy distribution $\omega\frac{dI}{d\omega}$ in the multiple soft scattering approximation for different values of the kinematic constraint $R = \omega_c\, L$=1000, 10000 and 40000.

of $R = \omega_c L$. A comparison with the BDMPS result is also shown. The origin of R is simple: as $k_t^2$ is limited by $\hat{q}L$, the upper kinematical limit in the $k_t$-integration cuts the gluon energies $\omega^2 \lesssim k_t^2 \sim \hat{q}L$. So, the spectrum is suppressed for

$$\left(\frac{\omega}{\omega_c}\right)^2 \lesssim \frac{2}{R}\,. \tag{7}$$

The position of the maxima is in agreement with this estimate. Thus, the suppression in the soft part of the spectra can be understood by formation time arguments. In this way, the fact that the radiation spectrum shows small sensitivity to the infrared region is ground on general arguments rather than on the actual realization of the model. This has important consequences in the experimental observables as we will see. The limit $R \to \infty$ is obtained by integrating the spectrum in $k_t^2 < \infty$,

$$\lim_{R\to\infty}\ \omega\frac{dI}{d\omega} = \int_0^\infty dk_t^2 \omega \frac{dI}{d\omega dk_t^2} = \frac{2\alpha_s C_R}{\pi}\,\mathrm{Re}\left[\ln\left(\cos\sqrt{\frac{\omega_c}{i\omega}}\right)\right] \tag{8}$$

which coincides with the BDMPS result[3]. The average parton energy loss is, then,

$$\langle \Delta E\rangle \equiv \int_0^\infty d\omega\, \omega \frac{dI}{d\omega} \quad \xrightarrow[R\to\infty]{} \quad \frac{\alpha_s C_R}{2}\,\omega_c \ \propto\ \hat{q}L^2\,. \tag{9}$$

This is the well-known $L^2$ dependence of the average radiative energy loss [3,4,5,6,7].

### 3.1. *Expanding medium*

The medium produced in a heavy ion collision is expanding very fast in the longitudinal and probably also in the transverse direction. The expansion is usually parametrized by an exponential decrease of the medium density as $n(\tau) \sim 1/\tau^\alpha$,

with $\alpha$=1 for 1-dimensional (Bjorken) expansion. In this case, the transport coefficient changes accordingly as $\hat{q}(\tau) = \hat{q}_0(\tau_0/\tau)^\alpha$ and the corresponding spectrum can be obtained from eq. (4). It has been found in Ref. [30] that any expanding medium can be related with a equivalent static one with effective transport coefficient

$$\bar{\hat{q}} = \frac{2}{L^2}\int_{\xi_0}^{L+\xi_0} d\xi\ (\xi - \xi_0)\ \hat{q}(\xi)\,. \tag{10}$$

This result confirms previous relations to the level of the average $\Delta E$ [31,32] and allows to use the static formulas for any expanding scenario.

## 4. Applications

Equation (4) has been calculated for the one-gluon inclusive case. Up to now no progress has been made in computing diagrams with more than one gluon emission, so, for practical applications one usually assumes the independent gluon emission approximation [33]

$$P_E(\epsilon) = \sum_{n=0}^{\infty}\frac{1}{n!}\left[\prod_{i=1}^{n}\int d\omega_i \frac{dI(\omega_i)}{d\omega}\right]\delta\left(\epsilon - \sum_{i=1}^{n}\frac{\omega_i}{E}\right)\exp\left[-\int d\omega \frac{dI}{d\omega}\right]\,. \tag{11}$$

In the case of small gluon multiplicities, the interference terms are expected to be small [33], and (11) should give a good approximation. For a medium of finite length $L$, there is a finite probability $p_0$ that no energy is lost – no gluon is radiated and the fragmentation is not affected. This discrete contribution decreases with increasing in medium path-length or increasing density of the medium. So, we write

$$P_E(\epsilon) = p_0\delta(\epsilon) + p(\epsilon)\,. \tag{12}$$

In Fig. 5 we plotted the discrete, $p_0$, and continuous, $p(\epsilon)$, contributions to the *quenching weights*, $P_E(\epsilon)$ for different values of $R = \omega_c\ L$.

### 4.1. *Inclusive particle production*

For high enough $p_t$ of the parton, the hadronization takes place outside the medium. In this case, the medium-modified fragmentation function is usually written as [34,35,30]

$$D_{k\to h}^{(\mathrm{med})}(z,Q^2) = \int_0^1 d\epsilon\, P_E(\epsilon)\,\frac{1}{1-\epsilon}\,D_{k\to h}(\frac{z}{1-\epsilon},Q^2)\,, \tag{13}$$

where $D_{k\to h}$ is the vacuum fragmentation function. The only effect of the medium in (13) is a shift in the energy of the initial parton given by $P_E(\epsilon)$. Additional (logarithmic) modifications in the $Q^2$-dependence are neglected, as they are subdominant as compared to $\epsilon = \Delta E/E \sim 1/Q$ (we identify $Q$ with the initial transverse energy of the parton $E$). In Fig. 6 the fragmentation functions for different media computed by (13) are compared to the corresponding vacuum case [30].

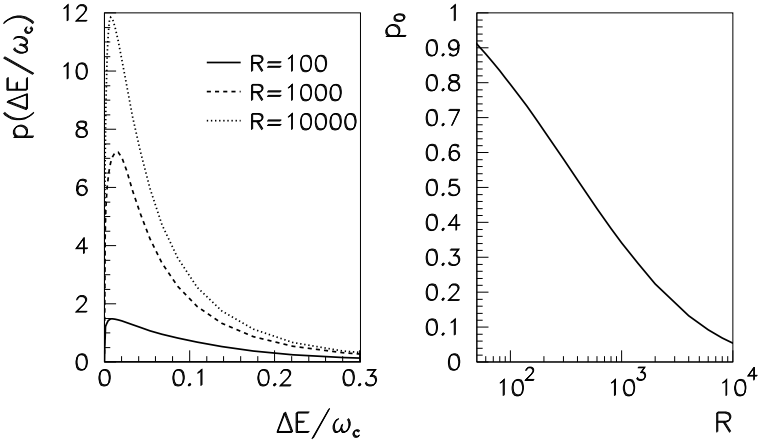


Fig. 5. The two contributions to the probability (11) that a parton loses $\Delta E$ of its energy in the medium: Continuous part (left panel) and the discrete probability $p_0$ in (12) that the hard parton escapes the medium without interaction (right panel).

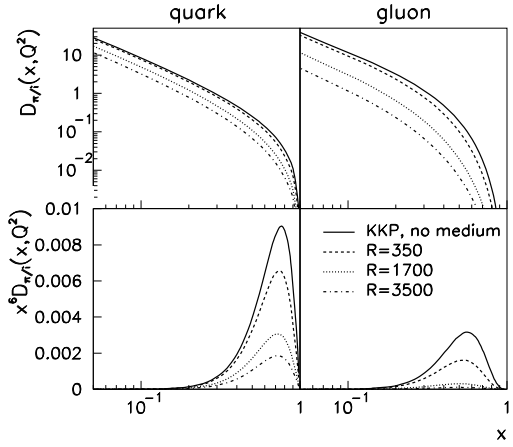


Fig. 6. Fragmentation functions for quarks and gluons into $\pi$ for media of different $R = \omega_c L$. The vacuum fragmentation functions are taken from [36].

In order to estimate the suppression of produced $\pi$'s we make use of the observation [15] that the partonic cross section and the PDF essentially contributes with $z^6$ to the integral in (1). In Fig. 6 we weight the fragmentation function by this factor, the ratios at the maxima between a medium and the vacuum gives the corresponding suppression of final $\pi$'s. A suppression by a factor of $4 \div 5$, as measured at RHIC, can be reached for R=1000 $\div$ 2000 (see also Fig. 7). These values are in agreement[30] with the ones obtained by the GLV group [32].

In order to study the sensitivity of these results to the small $\omega$-region, the so-

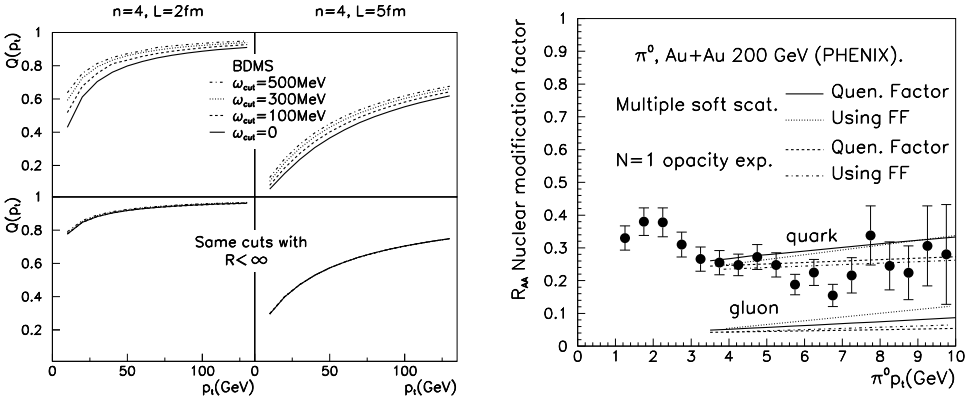


Fig. 7. LHS: Quenching factors (14) computed from the BDMPS spectrum (upper figures) and with finite R (lower figures) applying different cuts to the small-$\omega$ region ($\hat{q}$=1 GeV$^2$/fm has been taken). RHS: Comparison of the suppression obtained in the multiple soft and in the single hard scattering approximations with the experimental data from PHENIX [8] ($\omega_c$=67.5 GeV and R=2000 for both multiple soft and single hard scattering approximations).

called *quenching factors* have been introduced in Ref. [33],

$$Q(p_t) = \frac{d\sigma^{\rm med}(p_t)/dp_t^2}{d\sigma^{\rm vac}(p_t)/dp_t^2} = \int d\Delta E\, P(\Delta E) \left( \frac{d\sigma^{\rm vac}(p_t + \Delta E)/dp_t^2}{d\sigma^{\rm vac}(p_t)/dp_t^2} \right) , \qquad (14)$$

where the vacuum spectrum is usually taken as $d\sigma^{\rm vac}(p_t)/dp_t^2 \sim p_t^{-n}$. This can be seen as an alternative way of computing the effects of jet quenching. The sensitivity of the results to the infrared region can be studied by cutting-off the spectrum for $\omega \leq \omega_{\rm cut}$ and computing (14) – see Fig. 7. A strong sensitivity to the small-$\omega$ region appears when the BDMPS spectrum (8) is used [33,7]. With the regularization of the small$-\omega$ region due to finite $R = \omega_c L$, this sensitivity practically disappears [7]. In the RHS of Fig. 7 a comparison with PHENIX data of the suppression of $\pi^0$ for the most central AuAu collisions at RHIC is performed. The magnitude and the slope of the effect is in agreement with the data. This is in contrast with previous expectations based on BDMPS spectrum of a much steeper slope, see Fig. 7 (LHS). In this way, the results for the multiple soft and the single hard scattering approximations are similar.

### 4.2. *Jet shapes*

Equation (4) relates the energy loss of a parton with the transverse momentum broadening of the associated gluon radiation. This dynamics should modify the internal jet substructure from the vacuum case. In order to study these effects, a first attempt to compute jet observables in the presence of a medium has been made in [37]. In the rest of the section we present the medium–modification for two quantities, the fraction of jet energy inside a cone and the gluon multiplicity distribution.

The fraction of the jet energy inside a cone of radius $R = \sqrt{(\Delta\eta)^2 + (\Delta\Phi)^2}$ is

$$\rho_{\rm vac}(R) = \frac{1}{N_{\rm jets}} \sum_{\rm jets} \frac{E_t(R)}{E_t(R=1)} \,. \tag{15}$$

In the presence of the medium, this energy is shifted by[37]

$$\rho_{\rm med}(R) = \rho_{\rm vac}(R) - \frac{\Delta E_t(R)}{E_t} + \frac{\Delta E}{E_t} \left(1 - \rho_{\rm vac}(R)\right) \,, \tag{16}$$

where $\Delta E_t(R)$ is the additional (medium) energy radiated outside a cone $\Theta = R$ and $\Delta E(\Theta) = \int \epsilon P(\epsilon, \Theta) d\epsilon$, where the quenching weight is computed by integrating the spectrum (4) in $\omega \sin\Theta < k_t < \omega$. In Fig. 8 we plot the medium-shifted distributions. The shaded area corresponds to the uncertainty in finite quark-energy effects: in the eikonal approximation $P(\epsilon)$ have support in the unphysical region $\epsilon > 1$. To estimate this effect we make the change $P(\epsilon) \to P(\epsilon) / \int_0^1 d\epsilon P(\epsilon)$.

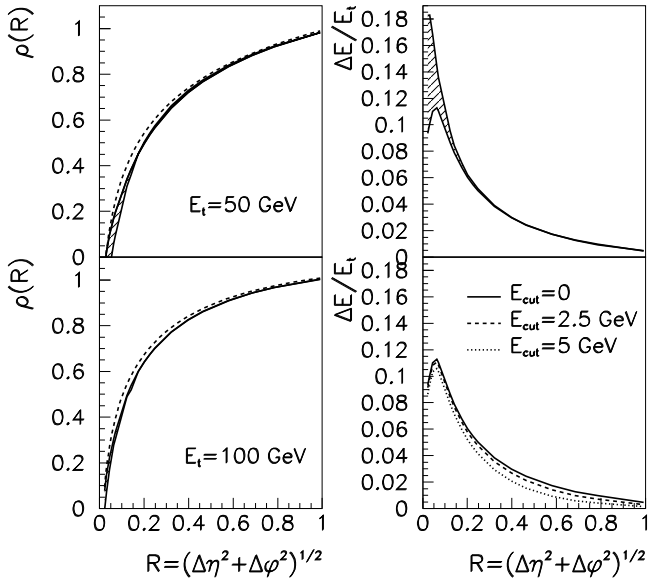


Fig. 8. LHS: The jet shape (15) for a 50 GeV and 100 GeV quark-lead jet which fragments in the vacuum [38] (dashed curve) or in a dense QCD medium (solid curve) characterized by $\omega_c = 62$ GeV and $\omega_c\, L = 2000$. RHS: the corresponding average medium-induced energy loss for $E_t = 100$ GeV outside a jet cone $R$ radiated away by gluons of energy larger than $E_{\rm cut}$. Shaded regions indicate theoretical uncertainties discussed in the text.

The effect of the medium is very small (at $R$=0.3, it is $\sim 5\%$ for a 50 GeV jet and $\sim 3\%$ for a 100 GeV jet). The smalleness of this effect could allow for a calibration of the total energy of the jet without tagging in a recoiling hard photon or Z-boson. It also implies that the jet $E_t$ cross section scales with the number of binary collisions. In order to check the sensitivity of our results to the small-energy

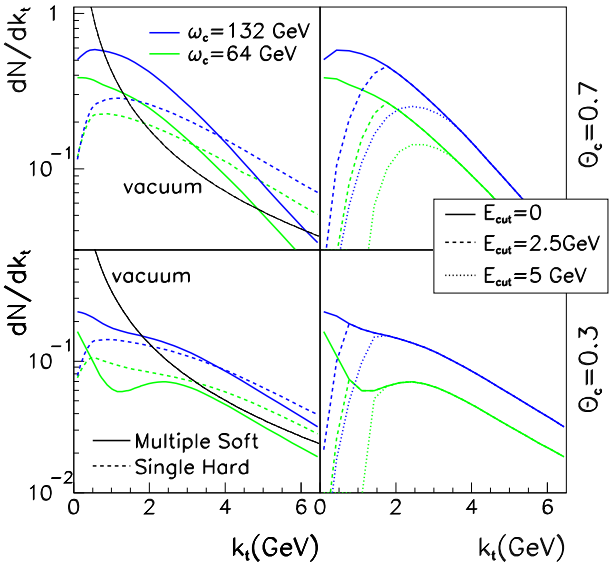


Fig. 9. Comparison of the vacuum and medium-induced part of the gluon multiplicity distribution (17) inside a cone size $R = \Theta_c$, measured as a function of $k_t$ with respect to the jet axis. Removing gluons with energy smaller than $E_{\rm cut}$ from the distribution (dashed and dotted lines) does not affect the high-$k_t$ tails.

region, we impose, in analogy to the previous section, low momentum cut-offs which removes gluon emission below 5 GeV. It is interesting that transverse momentum broadening is very weakly affected by these cuts. This is again due to the infrared behavior of the spectrum for small values of $\omega$ – see Fig. 4. A proper substraction of the large background present in heavy ion collisions would benefit from this result.

$k_t$-differential measurements are expected to be more sensitive to medium effects. As an example, the intrajet multiplicity of produced gluons as a function of the transverse (with respect to the jet axis) momentum is plotted in Fig. 9. The medium-induced additional number of gluons with transverse momentum $k_t = |\mathbf{k}|$, produced within a subcone of opening angle $\theta_c$, is

$$\frac{dN_{\rm med}}{dk_t} = \int_{k_t/\sin\theta_c}^{E_t} d\omega \, \frac{dI_{\rm med}}{d\omega \, dk_t} \, . \tag{17}$$

For the vacuum we simply assume $dN_{\rm vac}/dk_t \sim 1/k_t \log(E_t \sin\theta_c/k_t)$. In this case, the effect is sizable for transverse momenta of the order of several GeV and could be easily measured experimentally. A more realistic analysis would need of an implementation of the whole fragmentation. However, the origin of the shift is mainly due to the large $k_t \sim Q_{\rm sat}$ that the gluon obtains from the medium. In this way, we expect this conclusion to be very robust and not depending on the actual realization of the model.

## 5. Discussion and other approaches

In the previous sections, we have presented the usual framework to compute high-$p_t$ particle production in nuclear collisions. It is based on the collinear factorization, eq. (1), supplemented with nuclear parton distribution functions and final state effects due to medium-induced gluon radiation. This framework has been successfully employed to reproduce experimental data. Let us comment on the differences with other approaches within the same framework, concerning both the initial and the final state.

First, in the initial state intrinsic-$k_t$ and/or Cronin effect due to multiple (elastic) scattering are sometimes introduced (see e.g. [16,17,39]). The $p\bar{p}$ data cannot distinguish between these two approaches, however, $hA$ data at energies of several tens of GeV are well described with this mechanism. Its magnitude for central AuAu collisions at RHIC can be as large as a 50% increase. This increase is sometimes compensated by the large shadowing of Ref. [27], however, as we have seen this strong gluon shadowing is in disagreement with DIS data. The nuclear PDF obtained in a DGLAP analysis result only in a tiny enhancement [15,22].

Concerning the final state effects, most of the approaches rely on the radiative energy loss and differ only on the approximation used, multiple soft [3] or single hard scattering [5]. We have seen that both approximations give very similar results when the appropriate kinematical limits and correspondingly similar parameters are taken into account [7]. (For an approach based on twist expansion in DIS see Ref. [41]). The possibility of collisional energy loss has been also explored [40] with a reasonable result. As it has been exposed in Section 3, formation time arguments lead to a radiative energy loss which increases as $L^2$, in the case of a collisional energy loss the growth is, however, as $L$. So, the centrality dependence of the effect is expected to be sensitive to this different behavior. Unfortunately, it seems that present data cannot distinguish between a $L$ or $L^2$ behavior [42]. Notice that in all these analyzes, hadronization is assumed to take place outside the medium. This could not be the case for the smallest $p_t$ values [43].

On the other hand, an initial state origin for the suppression of high-$p_t$ particle production has been proposed in the framework of the saturation approach [44], the origin being the smaller number of initial gluons in the nuclei wave functions. There has been some discussion on whether this removes the Cronin enhancement at intermediate values of $p_t$ or not, but finally the different groups agree [45,46,47,48] in that saturation leads to a suppression for all values of $p_t$. $dAu$ experimental data ruled out this hypothesis as the main source of high-$p_t$ particle suppression at central rapidities. However the prediction is [45] that at higher energies and/or rapidities this mechanism very efficiently suppresses the high-$p_t$ particle yields. The new preliminary data from BRAHMS [49] find a strong reduction of $\pi$'s for $p_t < 2.5$ GeV in the forward direction. From the results in Section 2, a suppression like this seems difficult to accommodate in a DGLAP approach in collinear factorization. If this preliminary data is confirmed it could be the first clear indication of saturation

phenomena in nuclear collisions.

## 6. Conclusions

In this review we have described the most recent theoretical results relating medium-induced gluon radiation, energy loss and jet broadening. These effects are accessible for the first time in experiments of heavy ion collisions at RHIC. All the experimental data strongly point to a large jet suppression due to interaction with the produced medium. The larger energy of the LHC will allow for a qualitative new regime, where the jets are not completely suppressed and the jet substructure could be measured in the large background environment. This will open a completely new window for the study of the evolution of high energetic particles in a medium.

**Acknowledgments:** I would like to thank J. Albacete, N. Armesto, K. Eskola, H. Honkanen, V. Kolhinen, A. Kovner, V. Ruuskanen and U. Wiedemann for the very nice and fruitful collaboration which is partially reviewed in this paper. Critical reading of this manuscript by N. Armesto and U. Wiedemann is gratefully acknowledged.

1. J. D. Bjorken, Fermilab-Pub-82/59-THY, Batavia (1982); Erratum, unpublished.
2. M. Gyulassy and X.-N. Wang, Nucl. Phys. **B420** (1994) 583;
   X.-N. Wang, M. Gyulassy and M. Plümer, Phys. Rev. **D51** (1995) 3436.
3. R. Baier, Yu. L. Dokshitzer, S. Peigné and D. Schiff, Phys. Lett. **B345** (1995) 277;
   R. Baier, Yu. L. Dokshitzer, A. H. Mueller, S. Peigné and D. Schiff, Nucl. Phys. **B483** (1997) 291; R. Baier, Y. L. Dokshitzer, A. H. Mueller and D. Schiff, Nucl. Phys. **B531** (1998) 403.
4. B. G. Zakharov, JETP Letters **63** (1996) 952; ibidem **65** (1997) 615; Phys. Atom. Nucl. **61** (1998) 838 [Yad. Fiz. **61** (1998) 924]; JETP Lett. **70** (1999) 176; ibidem **73** (2001) 49.
5. M. Gyulassy, P. Levai and I. Vitev, Phys. Rev. Lett. **85** (2000) 5535 [arXiv:nucl-th/0005032]; Nucl. Phys. **B594** (2001) 371 [arXiv:nucl-th/0006010]; Phys. Rev. **D66** (2002) 014005 [arXiv:nucl-th/0201078].
6. U. A. Wiedemann, Nucl. Phys.**B588** (2000) 303 [arXiv:hep-ph/0005129]; Nucl. Phys. **A690** (2001) 731 [arXiv:hep-ph/0008241].
7. C. A. Salgado and U. A. Wiedemann, Phys. Rev. **D68** (2003) 014008 [arXiv:hep-ph/0302184]; Nucl. Phys. **A715** (2003) 783 [arXiv:hep-ph/0209025].
8. S. S. Adler *et al.* [PHENIX Collaboration], Phys. Rev. Lett. **91** (2003) 072301 [arXiv:nucl-ex/0304022]; D. d'Enterria [PHENIX Collaboration], Nucl. Phys. **A715** (2003) 749 [arXiv:hep-ex/0209051].
9. J. Adams *et al.* [STAR Collaboration], Phys. Rev. Lett. **91** (2003) 172302 [arXiv:nucl-ex/0305015]; G. J. Kunde [STAR Collaboration], Nucl. Phys. **A715** (2003) 189 [arXiv:nucl-ex/0211018].
10. I. Arsene *et al.* [BRAHMS Collaboration], Phys. Rev. Lett. **91** (2003) 072305 [arXiv:nucl-ex/0307003].
11. C. Adler *et al.* [STAR Collaboration], Phys. Rev. Lett. **90** (2003) 082302 [arXiv:nucl-ex/0210033].
12. S. S. Adler *et al.* [PHENIX Collaboration], Phys. Rev. Lett. **91** (2003) 072303 [arXiv:nucl-ex/0306021].

13. J. Adams *et al.* [STAR Collaboration], Phys. Rev. Lett. **91** (2003) 072304 [arXiv:nucl-ex/0306024].
14. B. B. Back *et al.* [PHOBOS Collaboration], Phys. Rev. Lett. **91** (2003) 072302 [arXiv:nucl-ex/0306025].
15. K. J. Eskola and H. Honkanen, Nucl. Phys. **A713** (2003) 167 [arXiv:hep-ph/0205048].
16. I. Vitev, arXiv:hep-ph/0212109.
17. P. Levai, G. Papp, G. G. Barnafoldi and G. Fai, arXiv:nucl-th/0306019.
18. A. D. Martin, R. G. Roberts, W. J. Stirling and R. S. Thorne, Eur. Phys. J. **C23** (2002) 73 [arXiv:hep-ph/0110215].
19. J. Pumplin, D. R. Stump, J. Huston, H. L. Lai, P. Nadolsky and W. K. Tung, JHEP **0207** (2002) 012 [arXiv:hep-ph/0201195].
20. K. J. Eskola, V. J. Kolhinen and P. V. Ruuskanen, Nucl. Phys. **B535** (1998) 351 [arXiv:hep-ph/9802350]; K. J. Eskola, V. J. Kolhinen and C. A. Salgado, Eur. Phys. J. **C9** (1999) 61 [arXiv:hep-ph/9807297]; K. J. Eskola, H. Honkanen, V. J. Kolhinen, P. V. Ruuskanen and C. A. Salgado, arXiv:hep-ph/0110348.
21. M. Hirai, S. Kumano and M. Miyama, Phys. Rev. **D64** (2001) 034003 [arXiv:hep-ph/0103208].
22. D. de Florian and R. Sassot, arXiv:hep-ph/0311227.
23. L. Frankfurt, V. Guzey, M. McDermott and M. Strikman, JHEP **0202** (2002) 027 [arXiv:hep-ph/0201230].
24. M. Arneodo *et al.* [New Muon Collaboration], Nucl. Phys. **B481** (1996) 23.
25. D. M. Alde *et al.*, Phys. Rev. Lett. **64** (1990) 2479.
26. K. J. Eskola, H. Honkanen, V. J. Kolhinen and C. A. Salgado, Phys. Lett. **B532** (2002) 222 [arXiv:hep-ph/0201256]; arXiv:hep-ph/0205231.
27. S. y. Li and X. N. Wang, Phys. Lett. **B527** (2002) 85 [arXiv:nucl-th/0110075].
28. Jan Czyzewski, K.J. Eskola, and J. Qiu, at the III International Workshop on Hard Probes of Dense Matter, ECT*, Trento, June 1995.
29. R. Baier, Y. L. Dokshitzer, A. H. Mueller, S. Peigne and D. Schiff, Nucl. Phys. **B484** (1997) 265 [arXiv:hep-ph/9608322].
30. C. A. Salgado and U. A. Wiedemann, Phys. Rev. Lett. **89** (2002) 092303 [arXiv:hep-ph/0204221].
31. R. Baier, Y. L. Dokshitzer, A. H. Mueller and D. Schiff, Phys. Rev. **C58** (1998) 1706 [arXiv:hep-ph/9803473].
32. M. Gyulassy, I. Vitev and X. N. Wang, Phys. Rev. Lett. **86** (2001) 2537.
33. R. Baier, Y. L. Dokshitzer, A. H. Mueller and D. Schiff, JHEP **0109** (2001) 033 [arXiv:hep-ph/0106347].
34. X. N. Wang, Z. Huang and I. Sarcevic, Phys. Rev. Lett. **77** (1996) 231.
35. M. Gyulassy, P. Levai and I. Vitev, Phys. Lett. **B538** (2002) 282 [arXiv:nucl-th/0112071].
36. B. A. Kniehl, G. Kramer and B. Pötter, Nucl. Phys. **B597** (2001) 337
37. C. A. Salgado and U. A. Wiedemann, arXiv:hep-ph/0310079.
38. B. Abbott *et al.* [D0 Coll.], FERMILAB-PUB-97-242-E.
39. I. Vitev and M. Gyulassy, Phys. Rev. Lett. **89** (2002) 252301 [arXiv:hep-ph/0209161].
40. M. G. Mustafa and M. H. Thoma, arXiv:hep-ph/0311168.
41. X. f. Guo and X. N. Wang, Phys. Rev. Lett. **85** (2000) 3591 [arXiv:hep-ph/0005044].
42. S. Y. Choi, M. Drees, B. Gaissmaier and J. Song, arXiv:hep-ph/0310284.
43. F. Arleo, JHEP **0211** (2002) 044 [arXiv:hep-ph/0210104].
44. D. Kharzeev, E. Levin and L. McLerran, Phys. Lett. **B561** (2003) 93 [arXiv:hep-ph/0210332].
45. J. L. Albacete, N. Armesto, A. Kovner, C. A. Salgado and U. A. Wiedemann,

arXiv:hep-ph/0307179.
46. R. Baier, A. Kovner and U. A. Wiedemann, Phys. Rev. **D68** (2003) 054009 [arXiv:hep-ph/0305265].
47. D. Kharzeev, Y. V. Kovchegov and K. Tuchin, arXiv:hep-ph/0307037.
48. J. Jalilian-Marian, Y. Nara and R. Venugopalan, arXiv:nucl-th/0307022.
49. R. Debbe, talk presented at the APS/DNP 2003, Tucson Arizona (2003), http://www4.rcf.bnl.gov/brahms/WWW/presentations.html.